The 2010 IEEE/RSJ International Conference on
Intelligent Robots and Systems
October 18-22, 2010, Taipei, Taiwan

Joint Mechanism with a Multi-directional Stiffness Adjuster

Shinya Kajikawa and Yasuo Yonemoto

Abstract— **This paper describes a novel joint mechanism with variable stiffness for a human-friendly robot. In the proposed mechanism, a set of two different hollow-shaped silicone rubber cushions (SRC$_{trans}$ and SRC$_{stiff}$: Silicone Rubber Cushion for transmission and for adjusting stiffness, respectively) are sandwiched between an output link and a motor-driven disk. SRC$_{trans}$, which is pressed against the motor-driven disk, plays the following three important roles: (1) it transmits rotational motion from the motor to the output link; (2) it absorbs excessive external forces by its elastic deformation and the slippage on the surface of the motor-driven disk; and (3) it allows the estimation of external forces using the information regarding the degree of deformation. On the other hand, SRC$_{stiff}$, which is placed below SRC$_{trans}$, controls the characteristics of joint compliance. SRC$_{trans}$ is pressed strongly against the motor-driven disk by the expansion of SRC$_{stiff}$. As a result, the output link can endure the external force without slippage. This paper describes the detail of joint structure and its fundamental performance.**

I. Introduction

A demand for human-care robots is growing with a rapid increase in the elderly population of our society. Human-care robots are expected to improve the quality of life of elderly or handicapped people by providing services to them. In human-care services, wiping and massaging human body or supporting rehabilitation will be one of essential tasks. While providing these services to them, these robots cannot avoid direct contact with human and will be exposed to external forces from multiple direction due to unpredictable human motion. Therefore, the working mechanism of these robots should be safe so as not to cause serious damage to humans, even if an unexpected collision occurs between humans and robots[1]. In addition, the robots should have the ability to adjust their characteristics depending on a given task and to generate dexterous motions.

In order to satisfy the abovementioned requirements for robot motion, the characteristics of joint compliance play important roles. Humans can generate many kinds of skillful motions by adjusting their joint characteristics to a desired task. As one of biological inspired mechanisms, a pneumatic artificial muscle systems emulating human muscular-skeleton structure have attracted considerable attention, and there have been many proposed mechanisms employing them [2][3][4]. In these mechanisms, the antagonistic arrangement of pneumatic artificial muscles is effectively used to independently control the joint position and joint compliance. Joint compliance can be adjusted by controlling the pressure in each muscle. However, a pneumatic muscle system has poor controllability in high frequency domain, because of its nonlinearity and a large dead time. Instead of pneumatic artificial muscles, two nonlinear spring systems(quadratic spring : $F(x) = x^2$) were employed in the antagonistic setup [5][6][7]. Quadratic springs in an antagonistic configuration provide a linear relationship between actuator co-contraction and joint stiffness. This is similar characteristics to biological joints, however, the drawback is the size, extra complexity, and friction of the mechanism to make the quadratic springs.

Other attractive approaches emplying a passive compliant element to control joint stiffness have been reported. Shin and Khatib[8][9] developed the Stanford Safety Robot which employs hybrid actuation, combining powerful pneumatic actuators with small electrical actuators in a parallel configuration at each joint. Iwata et al.[10] proposed a MIA (mechanical impedance adjuster) that employs a mechanically compliant leaf spring in the joint to maintain the link position. MIA can achieve ideal joint compliances by changing the length of the leaf spring. Kajikawa[11] inserted a CAP(compliance adjuster plate) between the joint and the link. Joint compliance can be adjusted by controlling the rotational position of the CAP around the principal axis of the link. Using this mechanism, fast arrangement of joint compliance within 200 ms can be achieved. Furthermore, other attractive compliant actuator designs are introduced in [12].

However above mechanisms can adjust the joint stiffness only along the rotational axis of the link. In actual contact with human, a contact point such as a robot arm will be exposed to external forces from multiple directions. Therefore we think that a robot joint should be designed to have a multidirectinal passive compliance and the ability to adjust it depending on a given task.

In this study, we propose a novel joint mechanism that involved the use of a motor and silicone rubber cushions (SRC); this mechanism gives a robot not only a multidirectional adjustable compliance but also controlability. In addition, it has the ability to sense external forces necessary for planning dexterous motion. In this mechanism, two different hollow-shaped cushions (SRC$_{trans}$ and SRC$_{stiff}$) are placed between a motor-driven disk and an output link. The friction force between the surface of SRC$_{trans}$ and the motor-driven disk helps in transimitting the rotational motion from the motor to the output link. In addition, SRC$_{trans}$ plays the following two important roles; (1) it absorbs external forces with slippage on the motor-driven disk and its elastic deformation and (2) it can estimate the direction and amplitude of external forces.

S.Kajikawa and Y.Yonemoto are with Department of Mechanical Engineering and Intelligent Systems, Faculty of Engineering, Tohoku Gakuin University, 9858537 Tagajo, Miyagi, Japan kajikawa@tjcc.tohoku-gakuin.ac.jp

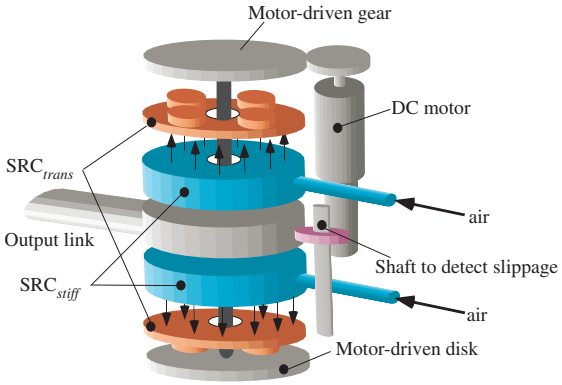

Fig. 1. Proposed joint mechanism. Expansion of SRC$_{stiff}$ presses SRC$_{trans}$ against the motor-driven gear and disk. The compression of SRC$_{trans}$ makes robot's joint stiffer.

On the other hand, SRC$_{stiff}$ controls the degree of pressing SRC$_{trans}$ against the motor-driven disk by its expansion. With an increase in the pressing force of SRC$_{trans}$, the joint endure a larger external force without slippage becuase of an increase in the static friction force between SRC$_{trans}$ and motor-driven disk. In other words, we can control the joint compliance by controlling the air flow into SRC$_{stiff}$. In the follwing section, we provide detail on the structure and fundamental performance of the proposed joint mechanism.

II. Proposed Mechanism

The proposed mechanism has a variable passive compliance against multidirectional external forces. In addtion, taking advantage of the elastic deformation of cushions, the direction and magnitude of the external forces can be easily estimated. The following section shows how a joint can achieve multidirectional passive compliance and estimate external forces.

A. Passive motion for safety

Fig. 1 shows the structure of the proposed joint mechanism. Two different types of air cushions, i.e., SRC$_{trans}$ and SRC$_{stiff}$ shown in Fig. 2, are employed in this mechanism. SRC$_{trans}$ consists of four small cushions, i.e., s-SRC$_{trans}$s, which are cylindrical in shape with a cavity. These cushions are placed on a concentric circle on the base plate of SRC$_{trans}$. On the other hand, SRC$_{stiff}$ has a simple doughnut shape. Two sets of SRC$_{trans}$ and SRC$_{stiff}$ are placed on the upper side and lower side of the output link, respectively, and they are sandwiched by the motor-driven gear and disk (see Fig. 1). These two cushions play different roles in the proposed joint mechanism.

Each s-SRC$_{trans}$ is in contact with the motor-driven gear or disk, and it transmits the rotational motion of the motor to the output link because of the friction torque between its surface and the motor-driven gear and disk. If the external force around the rotational joint axis, τ_x, is exerted on the output link, the shear deformation of s-SRC$_{trans}$ occurs. Then the external force becomes larger, the slippage between SRC$_{trans}$ and the motor-driven disk begins (see Fig. 3(b)).

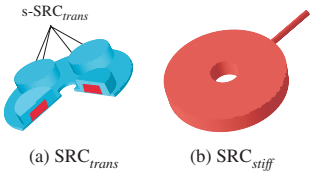

Fig. 2. Two cushions used in the proposed mechanism. (a) SRC$_{trans}$ consists of four s-SRC$_{trans}$s and is used to transmit the rotational motion from the motor to the joint shaft. (b) SRC$_{stiff}$ adjusts the characteristics of joint stiffness.

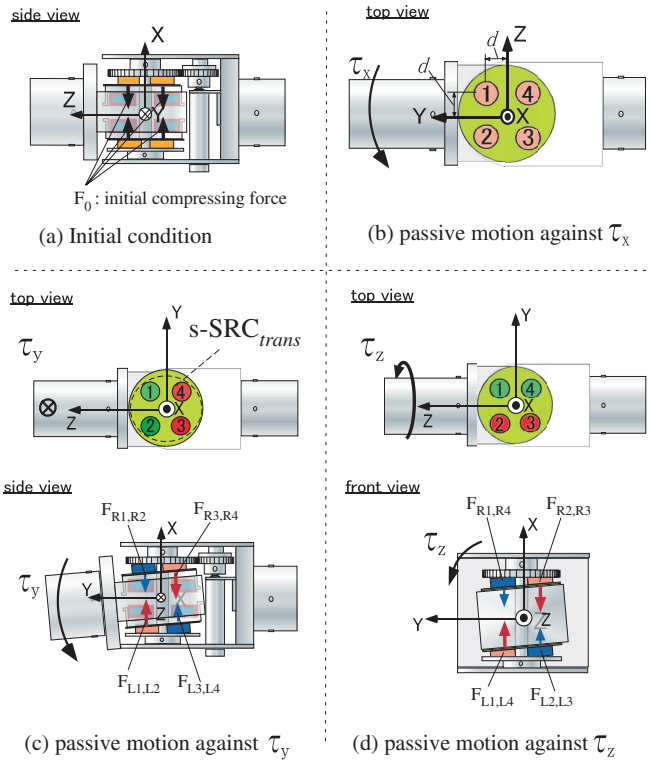

Fig. 3. Joint motion against external forces from multiple directions.

These phenomena absorb the excessive force and prevent the robot arm from causing a serious damage to human.

In addition, when the external forces around Y- and Z-axes, τ_y and τ_z, are exerted on the output link, they are also absorbed by the compressive deformation of s-SRC$_{trans}$. Therefore, we may can that this joint has a multidirectional passive compliance and guarantees safety and stable contact with human while performing their services.

On the other hand, SRC$_{stiff}$ aids in adjusting the joint stiffness. If SRC$_{stiff}$ is expanded by supplying air flow from a pump, each s-SRC$_{trans}$ will be strongly pressed against the motor-driven gear or disk. The joint becomes stiff and can endure larger external torque with the compression of s-SRC$_{trans}$, because the deformation of s-SRC$_{trans}$ is decreased and also the increment of friction force between s-SRC$_{trans}$ and the motor-driven disk restricts slippage. The detail of this phenomena is described in SectionIV.B.

B. Estimation of external forces

As described in the previous section, the joint can efficiently absorb external force because of the elastic defor-

mation and slippage of s-SRC$_{trans}$. The deformation and slippage causes backward rotation of the output link, and the link will behave like a spring until the beginning of the slippage. With regard to the external force around the joint axis, τ_x, we expect that the magnitude of the force can be estimated by measuring the difference of the position between the output link and the motor-driven disk. The angle of the motor-driven disk is measured using a potentiometer attached to the motor-driven shaft. On the other hand, actual position of the output link is known by measuring the angle of slippage detection shaft that contacts with the terminal part of the link and rotates together (see. Fig. 1).

On the other hand, the external torque around Y- and Z-axes, τ_y and τ_z, is also estimated using the information about the pressure in s-SRC$_{trans}$. As shown in Figs. 3(c) and (d), when τ_y or τ_z are applied to the output link, s-SRC$_{trans}$ numbered 1 and 2 or 3 and 4 are compressed, respectively. An increase in the compression force can be measured by the determining in the pressure of each s-SRC$_{trans}$. Furthermore, we determined which cushion was compressed to obtain the direction of the applied force.

Next, we explain the process of estimation of τ_y and τ_z. Initially, a compression force F_0 is exerted equally on all s-SRC$_{trans}$s because of their contact with the two motor-driven disks. Consider a situation in which τ_x, τ_y, and τ_z are applied simultaneously to the output link. Assuming that these torques, τ_x, τ_y, and τ_z, individually act on s-CushionAs as compressing force f^x, f^y, f^z, respectively. The magnitudes of the forces exerted on each s-SRC$_{trans}$, i.e., F_{Ri} and F_{Li}, are obtained as follows:

$$F_{Ri} = F_0 + f^x_{Ri} + f^y_{Ri} + f^z_{Ri}, \quad (1)$$
$$F_{Li} = F_0 + f^x_{Li} + f^y_{Li} + f^z_{Li}, \quad (2)$$

where the subscripts, R, L, and i (=1∼4) indicate the right and left side of the output link and the number of s-CushionA, respectively (see Fig. 3). The relationship between the external torques τ_y and τ_z and the forces exerted on the s-SRC$_{trans}$s, F_{Ri} and F_{Li}, is expressed as follows:

$$\tau_y = d(F_{R1} + F_{R2} - F_{R3} - F_{R4}) - d(F_{L1} + F_{L2} - F_{L3} - F_{L4}), \quad (3)$$
$$\tau_z = d(F_{R1} + F_{R4} - F_{R2} - F_{R3}) - d(F_{L1} + F_{L4} - F_{L2} - F_{L3}), \quad (4)$$

where d denotes the perpendicular distance from the center of each s-SRC$_{trans}$ to the Y- or Z-axis. On the basis of the symetrical arrangement of the s-SRC$_{trans}$s, the following relationship can be assumed:

$$f^x_{R_i} = f^x_{L_i} \qquad (i = 1 \sim 4), \quad (5)$$
$$f^y_{R_1} = f^y_{R_2} = f^y_{L_3} = f^y_{L_4}, \ f^y_{R_3} = f^y_{R_4} = f^y_{L_1} = f^y_{L_2}, \quad (6)$$
$$f^z_{R_1} = f^z_{R_4} = f^z_{L_2} = f^z_{L_3}, \ f^z_{R_2} = f^z_{R_3} = f^z_{L_1} = f^z_{L_4} \quad (7)$$

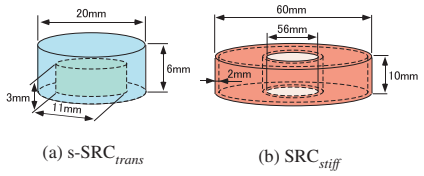

(a) s-SRC$_{trans}$ (b) SRC$_{stiff}$

Fig. 4. Dimensions of s-SRC$_{trans}$ and SRC$_{stiff}$.

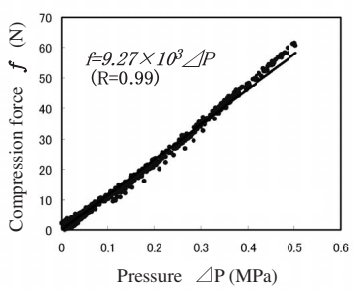

Fig. 5. Relationship between the compression force and the change in pressure.

Substituting Eqs. (1) and (2) into Eqs. (3) and (4), respectively, and also taking Eqs.(5)∼(7) into consideration, we obtain the following simple equations.

$$\tau_y = 2d(f^y_{R1} + f^y_{R2} - f^y_{R3} - f^y_{R4}) \quad (8)$$
$$= 4d(f^y_{R1} - f^y_{R3}), \quad (9)$$
$$\tau_z = 2d(f^z_{R1} + f^z_{R4} - f^z_{R2} - f^z_{R3}) \quad (10)$$
$$= 4d(f^z_{R1} - f^z_{R2}). \quad (11)$$

The above equations show that Eqs. (3) and (4) express the balance between the external torques τ_y and τ_z and the actual compression forces caused by each torque, f^y_{Ri} and f^z_{Ri}, respectively. Therefore, even if τ_x, τ_y, and τ_z are applied simultaneously, we can determine τ_y and τ_z individually by solving Eqs. (3) and (4), respectively. In addition, while calculating these torques, we find that the compression forces acting on either sides (left or right) are used only. Therefore, the actual equations for estimating the torques are given as follows:

$$\tau_y = 2d(F_{R1} + F_{R2} - F_{R3} - F_{R4}), \quad (12)$$
$$\tau_z = 2d(F_{R1} + F_{R4} - F_{R2} - F_{R3}). \quad (13)$$

F_{R1}∼F_{R4} can be easily determined by measuring ΔP in the s-SRC$_{trans}$s, as described in following section.

III. Prototype Joint Module

Figs. 6(a)(b) show a prototype planar 1-link arm system with the proposed joint module. The dimensions of the joint module are 130 mm × 72 mm × 82 mm, and its weight is approximately 1000 g. Its body is mainly made of aluminum and stainless steel. For the next version, we will modify the design and the materials used to develop a lighter module.

s-SRC$_{trans}$ and SRC$_{stiff}$ are made from silicone rubber (Shin-Etsu Chemical Co., Ltd: KE1300) and a thinner. The ratio of RTV (room temperature vulcanizing) silicone rubber

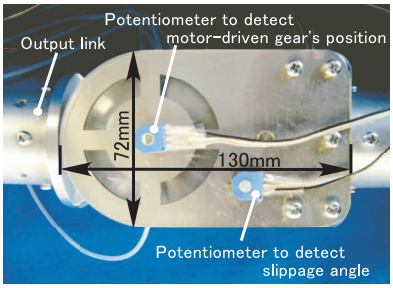

(a) Topview (outward appearance)

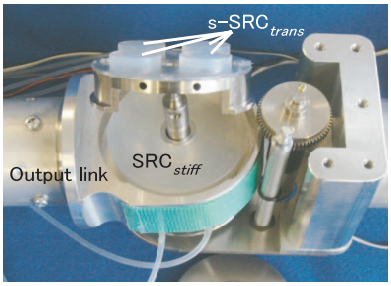

(b) Topview (inside the joint)

Fig. 6. Prototype joint module.

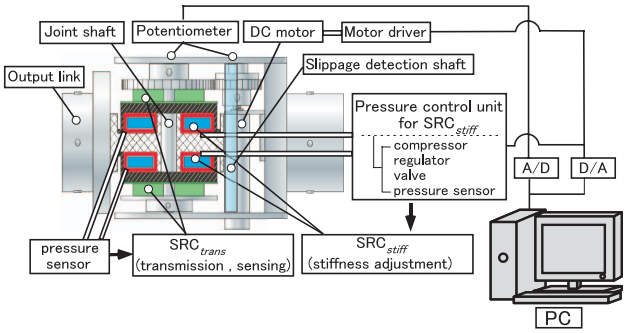

Fig. 7. Experimental setup.

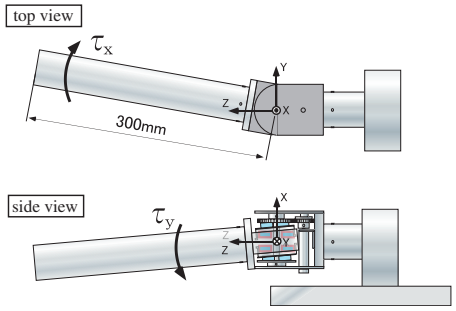

Fig. 8. 1-Link arm system with the proposed joint.

and the thinner is 9:1. Dimensions of these cushions are shown in Fig. 4. In the case of s-SRC$_{trans}$, the relationship between the compression force f and the pressure change in the cushion, ΔP, is shown in Fig. 5. This figure shows that the relationship between f and ΔP can be assumed to be linear ($f = 9.27 \times 10^3 \Delta P$). Using this relationship, we can estimate the amount of compression forces acting on each s-SRC$_{trans}$, F_{Ri} or F_{Li} (i = 1∼4), easily by measuring ΔP. From Eq.(1)∼ Eq.(13), it is known that torques τ_y and τ_z can be estimated by determining ΔP in each s-SRC$_{trans}$ only.

The proposed joint is actuated by a DC motor (STL JAPAN: HS-GM43-FPSL; maximum torque 0.98 Nm; rotational speed, 5∼22 rpm). The rotational motion of this motor is transmitted to the output link through the motor-driven gear, whose reduction ratio is 1:2. The rotational angle of the motor-driven gear and the output link are measured using two potentiometers (Murata Manufacturing Co., Ltd., SV01A103AE01), respectively.

The position of the output link can be known by measuring the position of slip detection shaft that makes a rolling contact to the terminal body of the output link. The difference of the positions between the motor-driven gear and the output link causes by the shear deformation of s-SRC$_{trans}$. So we can estimate the magnitude of the external torque, τ_x, with the gap between two positions.

In order to measure the pressure in the s-SRC$_{trans}$, four pressure sensors (Fujikura Ltd., PSM-050KPG, type: guage pressure, range: 0∼50KPa) are connected to four s-SRC$_{trans}$s attached to the upper side of the output link through silicone rubber tubes. This pressure information is used to detemine the contact situation of the link to the environment.

IV. Experiments

In this section, we show the basic performance and characteristics of the proposed joint module by performing several experiments.

A. Experimental setup

The experimental system is shown in Fig. 7. An output link, whose lenght and weight are 300 mm and 80 g, respectively, is attached to the prototype joint module. As shown in this figure, the pressure in SRC$_{stiff}$, P_b, is adjusted by a pressure control unit in order to achieve a desired joint compliance. This unit consits of an air compressor (Nitto Kohki Co., ltd.: DP0102H-X1; rated flow rate, 4.0 l/min; maximum pressure, 0.08 MPa), a flow regulator (SMC Corp.: ITV0031-3BS; regulating pressure range, 0.01∼0.1 MPa; maximum flow rate, 3.5 l/min), a flow valve (SMC Corp.: VX2110V-01-5G1-B; 2-port solenoid valve), and a pressure sensor(SMC Corp.: ISE90-C01-T-M; rated pressure range, -0.100∼1.000 MPa). This pressure control unit occupies only small space, therefore we would like to embed it into the upper arm body at next version.

On the other hand, the link motion is measured by two potentiometers(Murata Manufacturing Co., Ltd., SV01A10301) attached to the joint shaft and the slippage detection shaft, respectively.

B. Joint stiffness

First, we investigated the relationship between the pressure in SRC$_{stiff}$, P_b, and the joint stiffness K. In this experiment, we locked motor-driven gear and disk directly by thrusting a pin from the joint frame to them instead of locking DC motor, because we evaluate actual limitation of the joint stiffness.

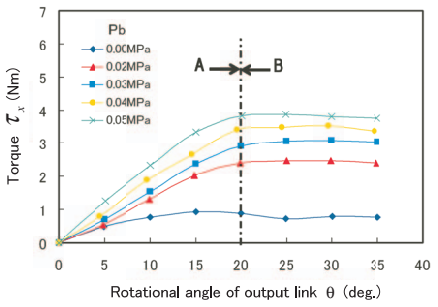

Fig. 9. Relationship between pressure in SRC$_{stiff}$ and joint stiffness.

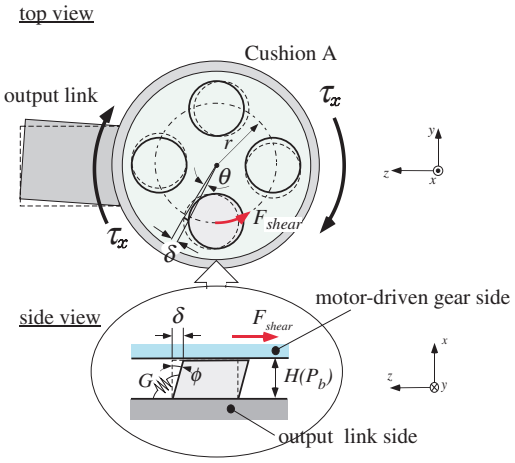

Fig. 10. Relationship between the deformation of SRC$_{trans}$ and the joint angle.

Then we pushed the output link, therefore the external force was mainly absorbed by s-SRC$_{trans}$s. We set the pressure in SRC$_{stiff}$ to 0.00, 0.02, 0.03, 0.04, and 0.05 MPa. At each pressure, we pushed the tip of the output link at a constant velocity of 5.0 mm/s using a force sensor around the X-axis and measured the reaction force during this process (see Fig. 8).

Fig. 9 shows the change in the reaction force (torque) for every approximately 5.0 deg. increase in the angle of the output link. When the pressure was 0.00 MPa, the link began to slip easily by a slight external torque, because s-SRC$_{trans}$s were not pressed firmly against the motor-driven gear and disk owing to an insufficient expansion of SRC$_{stiff}$.

Under other pressure conditions, we find that the link began to slip when its angle exceeds 20 deg. (Region B in this figure). In addition, the reaction torque at the beginning of slippage increased with the pressure P_b. In region A where the link endured the external torque, the relationship between the torque and the joint angle became almost linear.

Here we describe the reason why the joint behaves like a linear spring in region A. Fig. 10 shows the relationship between the angle of the output link, θ, and the deformation of s-SRC$_{trans}$s, δ.

As shown in this figure, when τ_x is applied on the link, a shearing force, F_{shear} acts on s-SRC$_{trans}$s and deforms them. We can define the height of s-SRC$_{trans}$ as a function of the pressure in SRC$_{stiff}$, P_b, because s-SRC$_{trans}$ is compressed by the expansion of SRC$_{stiff}$. Defining the height of s-SRC$_{trans}$ as $H(P_b)$, the deformation of s-SRC$_{trans}$ is expressed as follows,

$$\delta = H(P_b) \cdot \tan\phi \tag{14}$$

where $\tan\phi$ indicates the shear strain. Defining the shear modulus of s-SRC$_{trans}$ as G, the shear strain is described as

$$\tan\phi = \frac{F_{shear}}{G}. \tag{15}$$

From Eq.(14) and Eq.(15), the movement of the joint, θ caused by external torque,τ_x, is

$$\theta = \frac{\delta}{r} \tag{16}$$

$$= \frac{H(P_b)}{G \cdot r} F_{shear} \tag{17}$$

where r denotes the distance between the center of s-SRC$_{trans}$ and that of the joint. Eq.(17) means that the joint stiffness,K, can be defined as a function of the pressure in SRC$_{stiff}$,

$$\theta = \frac{1}{K(P_b)} \cdot F_{shear}. \tag{18}$$

From the experimental results shown in Fig.9, we can obtain the joint stiffness $K(P_b)$ as $K(P_b) = 3.06P_b + 0.068$ (Nm/deg.) (see Fig. 11).

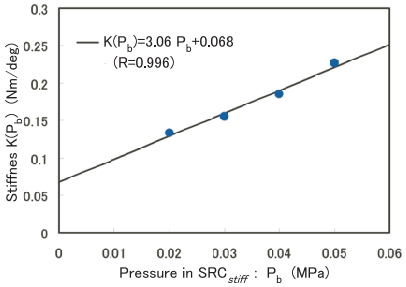

Fig. 11. Relationship between joint stiffness and pressure in SRC$_{stiff}$

C. Absorption of impact force

We examined the reaction of the joint module to the external force applied suddenly on the link during its movement and evaluted its effectiveness to soften the shock. We let the link collide with a force sensor and measured the impact force. The link is made from aluminum; therefore, we can assume that collision occurs between two rigid objects, in which the contact force can not be absorbed by the sensor or the link body.

The pressure in SRC$_{stiff}$, P_b, was set to 0.0 MPa and 0.05 MPa. Furthermore, a weight of 200 g was mounted on the link to increase the inertia of the link. Its mounted point was 250 mm away from the center of the rotation of the link. Collision with the force sensor occurred while the link rotates with a constant velocity of 60 deg/s. The contact point on the link was located 200 mm away from the rotational axis of the link.

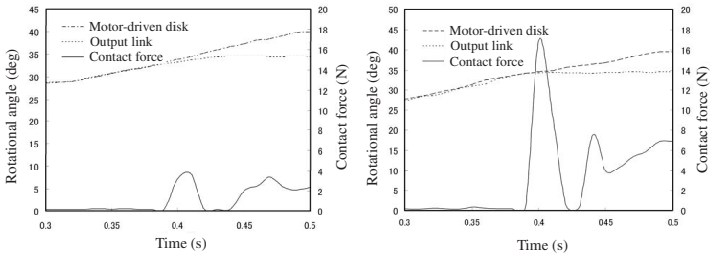

(a) P_b=0.00 MPa (b) P_b=0.05 MPa

Fig. 12. Comparison of impact forces.

Figs. 12(a)(b) show the experimental results. As shown in Fig. 12(b), the maximum of impact force is 17.9 N. At the moment of contact, the slippage between the link and the motor-driven disk did not occur, because s-SRC$_{trans}$s were adhered strongly to the disk.

On the other hand, when P_b was 0.0 MPa, the peak of impact force was reduced to 4.0 N. In this case, large slippage occurred easily between the output link and the motor-driven disk, which resulted in an effective absorption of the impact force.

From the comparison of the two results, we confirmed that a wide adjustable range of stiffness of the joint can be obtained by controlling P_b.

D. Controllability

In this section, we investigate the controllability of the joint module by performing several experiments. There is a possibility that s-SRC$_{trans}$ degrades the control performance under fast motion becuase of its elastic deformation and slippage.

At first, we investigated the frequency response of the joint by inputting a sinusoidal signal with an amplitude of $\pm$20deg. into DC motor. In this experiment, the pressure in SRC$_{stiff}$, P_b, was set to 0.00 MPa. Under this condition, the output link became slippy and the controllability would worsen compared to other pressure condition. The position of the output link was measured with the potentiometer attached to the slippage detection shaft. Comparing the position of the output link with that of the DC motor, we calculated the gain and phase parameters, respectively.

As the result, under the worst condition, the joint could follow perfectly the motion of DC motor less than 1.25Hz.

In second experiment, we applied a sinusoidal input with an amplitude of $\pm$15 deg. and synchronized the motion of DC motor with it. The frequency of the input signal was 1.5 Hz. Furthermore, we mounted a weight of 300 g on the output link at a position of 250 mm away from the center of the joint.

The joint stiffness could be adjusted by setting the pressure in SRC$_{stiff}$ to 0.00 MPa and 0.05 MPa. Figs.13(a)(b) show the experimental results. From these results, we confirmed that the output link could follow a desired position without perfect slippage. However, the amplitude of the output link tended to be greater than that of the motor-driven gear because of the elastic deformation of s-SRC$_{trans}$ caused by

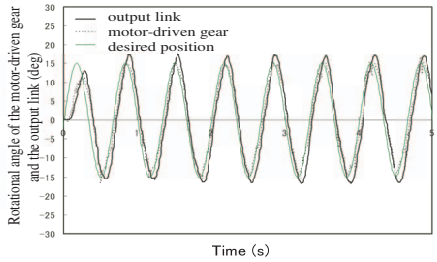

(a) P_b = 0.00 MPa

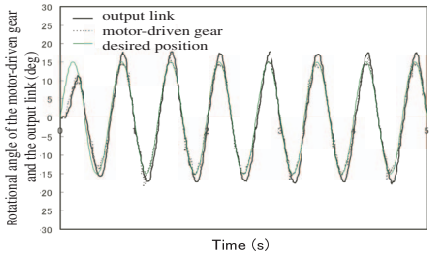

(b) P_b = 0.05 MPa

Fig. 13. Comparison of tracking performances for sinusoidal motion.

the inertia of the weight. In addition, as shown in Fig. 13(a), when the joint stiffness was not sufficient, we found that the output link was slightly delayed. It was easy to deform s-SRC$_{trans}$ along the rotational direction of the motor-driven disk, which caused the delay of the output link.

On the other hand, if s-SRC$_{trans}$ was compressed firmly, the delay was decreased sufficiently because it became difficult to deform s-SRC$_{trans}$ along the shearing direction (around X-axis).

E. Force estimation

Finally, we demonstrate the ability of the joint to estimate external forces. As one of the examples, the result of the estimation of the external force around Y-axis, τ_y, is shown here. τ_y was applied by pushing the link with a finger. The pushing force was measured using the force sensor attached to the fingertip. We set the pressure in SRC$_{stiff}$, P_b, to be 0.01 MPa and 0.05 MPa in order to examine the influence of the joint stiffness on the estimation performance.

Figs. 14 and 15 show the experimental results obtained when P_b was 0.01 MPa and 0.05 MPa, respectively. From these results, we found that the joint could accurately estimate the force even if the degree of compression of s-SRC$_{trans}$s differs because of the pressure in SRC$_{stiff}$, P_b. In the estimation argorithm, we did not use the value of pressure in s-SRC$_{trans}$ but its change in order to estimate the external forces τ_y and τ_z.

On the other hand, the external force around the X-axis, τ_x, could be estimated correctly before the begining of slippage by measuring the difference between the output link and the motor-driven disk , because the relationship between the difference and τ_x becomes linear as a spring as shown in Fig. 9. If we glue the surface of s-SRC$_{trans}$ to the motor-driven gear, the slippage will be prevented and the estimation of τ_x will become easier.

V. DISCUSSION

In this paper, we described a novel joint mechanism with variable compliance, and we investigated the fundamental features of the characteristics of passive compliance, controllability, and ability of sensing external forces.

First, we confirmed that joint compliance can be adjusted easily by controlling the pressure in SRC$_{stiff}$, P_b, and the adjustable compliance ranged from 0.068 Nm/deg to 0.22 Nm/deg, while P_b is controlled from 0.0 MPa to 0.05 MPa. The output link moves slowly, as if it is supported by a spring, while the difference of the position from the motor-driven disk is less than 20deg. This prototype joint has good characteristics in terms of soft compliance; however, in an actual case such as transporting a heavy load, the robot should firmly endure the external force. In order to increase the stiffness to a higher level, we need to set a higher pressure P_b or to modify the design and the material of s-SRC$_{trans}$.

Second, with regard to controllability, the output link could follow a sinusoidal motion of 1.25 Hz perfectly. Even if the weight of 300g was mounted on the tip of the link, the joint could follow the desired motion (its amplitude and frequency were $\pm$15deg. and 1.5Hz, respectively) without a fatal error and delay. The error and delay tended to increase with a decrease in the stiffness. We confirmed that a decrease in the performance was attributed to the elastic deformation of s-SRC$_{trans}$, and not to the slippage. In order to solve this problem, we have to use a robust controller considering the dynamics of s-CushionA to this joint system.

Finally, the ability to estimate the contact force was investigated in Section IV-E. The results indicated that the joint could estimate the force correctly, even if it changed dynamically. The estimation algorithm has two features: (1) it is very simple and (2) only the information regarding the pressure in s-SRC$_{trans}$ is used. Therefore, the estimation can be completed within a short time and is robust against electrical noise.

VI. CONCLUSION

In this study, we proposed a novel joint mechanism to achieve variable stiffness. In this mechanism, two different types of silicone rubber cushions are effectively used. Taking advantages of the elasticity of the cushions, the absorption of external forces from multiple directions and the estimation of the magnitude and direction of external forces are carried out. From the results of several experiments, we confirm that the proposed joint can give a robot the possibility to generate a skillful and gentle motion.

VII. ACKNOWLEDGMENTS

This work was partially supported by Electro-Mechanic Technology Advansing Foudation and a Grant-in-Aid for Scientific Research (#21560268) from the Japan Society for the Promotion of Science.

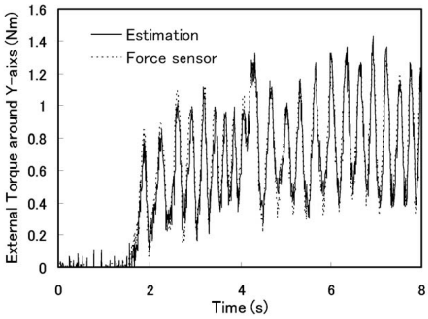

Fig. 14. Estimation result (Pressure in SRC$_{stiff}$: 0.01 MPa)

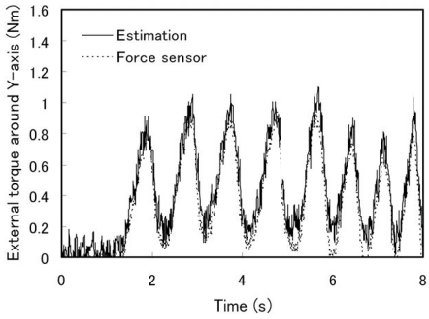

Fig. 15. Estimation result (Pressure in SRC$_{stiff}$: 0.05 MPa)

REFERENCES

[1] A.Bicchi and G.Tonietti, Dealing with the safety-performance tradeoff in robot arms design and control-fast and soft-arm tactics, *IEEE Robotics and Automation Magazine, 11*, 2004, 22-33.

[2] T.Noritsugu and T.Tanaka, Application of rubber artificial muscle manipulator as a rehabilitation robot, *IEEE/ASME Trans. on Mechatronics, 2*, 1997, 259-267.

[3] N.Saga and T.Saikawa, Flexor mechanism of robot arm using pneumatic muscle actuators, *Proc. of IEEE Int. Conf. on Mechatronics and Automation*, 2005, 1261-1266.

[4] B.Tondu, S.Ippolito, J.Guiochet, and A.Daidie, A seven-degrees-of-freedom robot-arm driven by pneumatic artificial muscles for humanoid robots, *Int. J. Robotics Research, 24(4)*, 2005, 257-274.

[5] S.A.Migliore, E.A.Brown, and S.P.DeWeerth,Biologically inspired joint stiffness control, *IEEE Int. Conf. on Robotics and Automation*, 2005, 4519-4524.

[6] K.Koganezawa, T.Inaba, and T.Nakazawa, Stiffness and angle control of antagonistically driven joint, *IEEE/RAS-EMBS Int. Conf. on Biomedical Robotics and Biomechatronics*, 2006,1007-1013.

[7] C.English and D.Russell, Mechanics and stiffness limitations of a variable stiffness actuator for use in prosthetic limbs,*Mechanism Mach. Theor.,34(1)*, 1999, 7-25.

[8] D.Shin, I.Sardellitti, and O.Khatib, A hybrid actuation approach for human-friendly robot design, *Proc. of IEEE Int. Conf. on Robotics and Automation*, 2008, 1747-1752.

[9] D.Shin, O.Khatib, and M.Cutkosky, Design methodologies of a hybrid actuation approach for a human-friendly robot, *Proc. of IEEE Int. Conf. on Robotics and Automation*, 2009, 4369-4374.

[10] H.Iwata, H.Hoshino, T.Morita, and S.Sugano, A physical interference adapting hardware system using MIA arm and humanoid surface covers, *Proc. of IEEE/RSJ Int. Conf. on Intelligent Robots and Systems*, 1999, 1216-1221.

[11] S.Kajikawa, Development of a robot hand with an adjuster mechanism for joint compliance, *Proc of IEEE Int. Conf. on Robotics and Biomimetics*, 2008, 1683-1688.

[12] R.Ham, T.Sugar, B.Vanderborght, K.Hollander, and D.Lefeber, Compliant actuator designs, *IEEE Robotics and Automation Magazine,16(3)*, 2009, 81-94.